Physica B: Condensed Matter 555 (2019) 21–31

Contents lists available at ScienceDirect

Physica B: Condensed Matter

journal homepage: www.elsevier.com/locate/physb

Analysis of oxygen bonding with metals of different oxidation states from experimental charge density distribution

K. Sujatha[a,b], S. Israel[b,*], C. Anzline[a,b], K.S. Syed Ali[c], R.A.J.R. Sheeba[d], P. Richard Rajkumar[b]

[a] *Mother Teresa Women's University, Kodaikanal, 624 102, Tamil Nadu, India*
[b] *Department of Physics, The American College, Madurai, 625 002, India*
[c] *Department of Science, Harmony Science Academy, Dallas, TX 75243, USA*
[d] *Department of Physics, The Madura College, Madurai, 625 011, India*

ARTICLE INFO

Keywords:
Charge density
Multipole model
MEM model
Bond critical points
Intermediate interactions
Strong correlation induced interactions

ABSTRACT

Oxygen bonding with metals of different oxidation state of metal cations, ranging from +1 to +6 have been thoroughly analysed using experimental charge density distribution evolved from X-ray diffraction experiments using multipole and MEM models of charge density. Oxygen atoms enacting different bonding characteristics at different symmetries are well defined in the course of study of the (3,-1) bond critical points. In case of low oxidation state of metal cations, as viewed in SrO and ZnO, ionic interactions are pronounced. As the oxidation on metals ascend, combinations of intermediate, polar covalent and eventually strong correlation induced interactions are evidenced.

1. Introduction

Nature has blessed the scientific community with a vast range of functional and exotic oxides, with fascinating physical, chemical, mechanical, optical, electrical and electronic properties, which could be considered as potential candidates for many brilliant applications such as heterogeneous catalysts, transparent conductors, gemstones, fuel cells, smart sensors and display devices to name just a few [1–7]. Literally, oxides are binary compounds that contain at least one oxygen atom and one other element in its chemical formula. Since oxygen is the second highest electronegative element [8], this ligand has the ability to form stable chemical compounds with almost all elements in the periodic table to give the corresponding oxides. For the convenience of understanding the electronic structures and the phenomenal and wide range of properties of binary oxides, a useful distinction between the oxides, in which the cation valence orbitals are of s or p character, viz Non-transition metal oxides and those in which the cation valence orbitals have d symmetry, viz Transition metal oxides, exist. The non-transition metal oxides are further classified as Pre-transition metal oxides and Post-transition metal oxides. Both the alkali metal oxides and the alkaline earth oxides constitute the pre-transition metal oxides [9,10].

As a matter of fact, almost all the properties of the materials are driven mainly by its bonding motifs [11]. Linus Pauling in 1929 [12], introduced two parameters, viz, bond ionicity and bond strength for the purpose of categorizing bonds in solid state. Later, the scale of electronegativity, introduced by Pauling, has become the most widely used parameter to differentiate the ionic and covalent bonds in solids [8]. The concept is that, as the electronegativity difference Δ, between the cation and anion increases, the ionic character of the bond also increases. Based on Pauling's electronegativity scale, several researchers (Mulliken [13,14], Allred and Rochow [15], Allred [16], Sanderson [17,18], Allen [19], Hohenberg and Kohn [20], Parr and Weitao Yang [21]) have developed various commonly used experimental and theoretical scales. Despite an adequate number of the concepts and parameters reported, two opposite views coexist between the researchers in rationalizing the bonding characteristics of binary oxides. One is that, the arguments based on the electron affinity scales and acidity scales could be extended to binary oxides and is shown to be energetically favourable for the purpose, e.g., Lenglet [22] and Duffy [23]. Other arguments, in contrast, controversially conclude that these parameters are less useful for the description of bonding motifs in oxides, since it exhibit ionic-covalent character of interatomic interaction. Concomitant with this view, Idriss et al. [24] have emphasized the parameter, chemical hardness and Andrzej Stoklosa [25] has emphasized molar volume for relating the properties of the binary oxides and hence to predict the trend of bonding character in iono-covalent oxides. Even though this dispute continues, almost all the studies on oxides reported in literature have stressed certain common points. That is, the most important concept of oxidation state, and also the position of the metal

---

[*] Corresponding author.
E-mail address: israel.samuel@gmail.com (S. Israel).

https://doi.org/10.1016/j.physb.2018.12.005
Received 12 March 2018; Received in revised form 15 November 2018; Accepted 2 December 2018

cation in the periodic table, matter the bonding principles of binary oxides [1,2,25–28].

The desire of oxygen ions in crystal structure to achieve a closed shell $2s^22p^6$ electronic configuration, tend them to form as O^{2-} anions, and thus they exist in an oxidation state of −2 in all metal oxides except peroxides and superoxides [10,23]. In general, the oxidation state of cations in binary oxides ranges from +1 to +8. In case of pre transition metal oxides, the cations in alkali metal oxides exist in +1 oxidation state and those in alkaline earth oxides exist in +2 oxidation state. Numerous theoretical and experimental works have outlined that the bonding in M_2O and MO oxides are predominantly ionic [10,26,28]. In case of post-transition metal oxides, the most important Binary Metal Oxides (BMOs) can have +3 valence. But exceptions are there, for example Zn ion exists in +2 valence state and Sn ion can have either a +2 or +4 valence [10,23]. According to Victor E. Henrich et al. [9], compared with alkaline earth oxides, the post-transition metal oxides exhibit a low ionic character of bonding, perhaps it exhibit covalent character of bonding [10]. The most striking feature of Binary Transition Metal Oxides (BTMOs) is that the cations can have a variety of stable oxidation states. One such example is manganese which has stable valence states of +2, +3, +4, +6 and + 7 [10,29]. Regarding these BTMOs, Victor E. Henrich et al. [10] predict a covalent type of bonding, but conversely, S.K.Deb [6] predicts an ionic type of bonding. In addition to this, a few literature predict an iono-covalent type of bonding [22,25,28]. In spite of all these data, some works have reported that the bonding in BMOs and BTMOs can vary from ionic to covalent [5,27]. These reports underline the need to document the degree of ionicity and the extent of covalence mixing in metal oxides.

Charge density is a versatile tool which has the ability to do an obvious work of providing an analytical description of the electronic structures, properties, chemical bonding and the correlations between them, in a compound. As a consequence, Israel et al. [30] have undergone a charge density study in some of the pre-transition metal oxides and arrived at a complete analysis of the strength of ionicity in bonding between the metal and oxygen atoms. With these motivations, we have embarked on an experimental charge density study of the structural and bonding properties of some transition and later transition metal oxides at different oxidation states of metals viz, (i) ZnO, for +2 oxidation state of metal, (ii) Al_2O_3, for +3 oxidation state of metal, (iii) ZrO_2, for +4 oxidation state of metal, (iv) V_2O_5, for +5 oxidation state of metal and (v) $WO_3 \cdot \frac{1}{3}\ H_2O$, for +6 oxidation state of metal.

Knowledge of the crystal structures is a prerequisite for understanding the properties, especially the bonding characteristics of oxides [9,31]. Binary oxides, in general, adopt diverse structures [25,29,32–34], which include (i) Halite (MgO, CaO, BaO), (ii) Cuprite (Cu_2O), (iii) Wurtzite (BeO), (iv) Massicot (β-PbO), (v) Corundum (Fe_2O_3, Cr_2O_3), (vi) Rutile (TiO_2, SiO_2, SnO_2), (vii) Baddeleyite (ZrO_2), (viii) Spinel (Mn_3O_4, Fe_3O_4, Co_3O_4), (ix) Rocksalt (MnO, FeO, CoO) and (x) Fluorite structures (HfO_2). In some cases, other structures also exist such as orthorhombic (V_2O_5) and monoclinic (CuO). In this regime, ZnO, the subject of this study for +2 oxidation state of metal, crystallizes in wurtzite structure based on the space group $P6_3mc$ [35–37]. This structure can be described as a number of Zn and O ionic planes stacked alternatively along the c-axis of the hexagonal symmetry. The most stable structure of Al_2O_3, which is the second subject of this study for +3 oxidation state of metal, is corundum with $R\bar{3}c$ space group symmetry [38–41]. Each aluminum atom is surrounded by six oxygen atoms and each oxygen atom is surrounded by four aluminium atoms. The baddeleyite phase of zirconia in which zirconium exists in +4 oxidation state, has a monoclinic structure with $P2_1/c$ space group [42–44]. Each Zr atom is connected to two oxygen sites, O1 and O2 with a coordination number of seven (i.e. three O1 and four O2 atoms). Each O1 ligand is connected to three Zr atoms whereas each O2 ligand is connected to four Zr atoms. Vanadium pentoxide, in which vanadium exists in +5 oxidation state, forms an orthorhombic crystal with *Pmmn* space group [45–48]. Here the vanadium atoms are bonded to three oxygen sites with a coordination number of five (i.e. one vanadyl oxygen atom (O1), one bridging oxygen atom (O2) and three O3 atoms). Each vanadyl oxygen atom, bridging oxygen atom and O3 atom is bonded to one, two and three vanadium atoms respectively. Limited theoretical and experimental works on tungsten trioxide hydrate $WO_3 \cdot \frac{1}{3}\ H_2O$ has gained substantial interest to choose this material for the study of oxide in +6 oxidation state of the metal. This hydrate has orthorhombic symmetry with *Fmm*2 space group [49,50]. There are two structurally different tungsten atoms (W1 and W2) and five structurally different oxygen atoms (O1, O2, O3, O4, and O5). Each W1 atom is coordinated to two O1 atoms, two O2 atoms and two O3 atoms whereas each W2 atom is coordinated to four O2 atoms, one O4 atom and one O5 atom. According to Gerand et al. [49], O4 is a water molecule. Only few theoretical and experimental charge density studies have been done for these materials [36,38,39,48,51–54] and moreover, the information available regarding the bonding principles is both incomplete and not well verified. And also, interestingly, there are no reports of charge density studies on $WO_3 \cdot \frac{1}{3}\ H_2O$. Hence extensive experimental charge density research efforts are focused to elucidate and compare the bonding mechanisms in these binary oxides which exist in different oxidation states of metals.

2. Sample and data collection

Highly pure (99.99%) commercially available powders of the above said chosen materials were used in this work. The powder X-ray diffraction data for these samples were collected using Bruker X-ray diffractometer of D8 advanced ECO XRD system with SSD160 1 D Detector. MoK_α wavelength of 1.54060 Å was used with a 2θ range from 5° to 120° in steps of 0.01° interval. The obtained X-ray diffractograms were compared and matched with Joint Committee Powder Diffraction Standards (JCPDS) data. The absence of additional peaks confirms the good quality of data.

3. Structure refinement using rietveld technique

To extract the structural details and structure factors, the raw XRD profiles were subjected to Rietveld refinement analysis [55] using the software JANA 2006 [56], which is a standard tool devised by Hugo Rietveld for the characterization of crystalline materials. This method adopts the principle of minimizing the difference between the theoretically modeled profile and the observed ones as a function,

$$D = \sum_{hkl} W_{hkl}(|F_O| - |F_C|)^2$$

Here the weight to be assigned to an observation is designated as W_{hkl} and the observed and calculated structure factors are designated as F_O and F_C respectively. In this technique, scale, structural parameters, lattice parameters, peak shift, preferred orientation, background profile functions, thermal parameters, surface roughness were refined until the observed XRD profile matches well with the calculated profile.

The profiles of all the five samples thus refined showed perfect fitting. The fitted powder profile of ZnO is presented as Fig. 1 as an example. The resultant refined parameters and reliability indices are tabulated as Table 1. The low R-factors in the table indicates the accuracy of the data and successful refinements. The structure factors and the thermal parameters extracted from these refined profiles were further utilized for the estimation of accurate charge density in the unit cells of these binary oxides.

4. Charge density analysis

In this work, for predicting the trend of bonding character in the samples, the most appropriate electron density distribution was constructed by using two best possible mathematical tools, multipole and maximum entropy method.

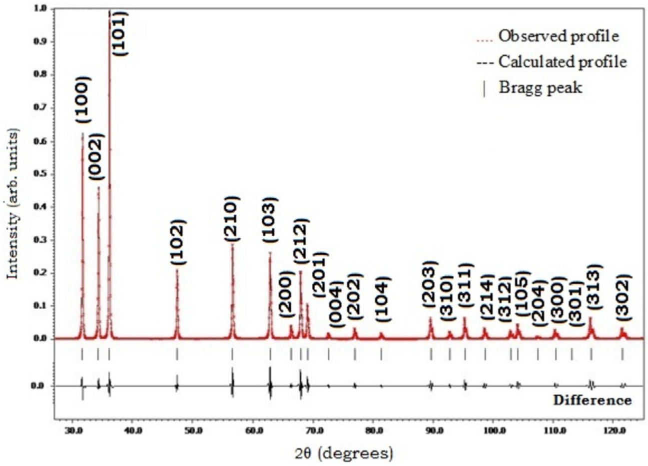

Fig. 1. Rietveld refinement profile of ZnO.

4.1. Multipole analysis

For understanding the charge distribution in a crystal, it is necessary to study the intricate details of the charge related parameters including the contraction/expansion of atoms in the systems. This can be achieved by constructing the electron density model proposed by Hansen and Coppens [57] which allows the refinement of population parameters at different orbital levels. In this model, the charge density, defined as,

$$\rho(r) = \sum_{k}^{atoms} \rho(r - r_k - u) \otimes \ t_k(u),$$

where $t_k(u)$ is the Gaussian term and the symbol $\otimes$ represents the convolution, is the superposition of harmonically vibrating aspherical atomic density distribution and each atomic density defined as,

$$\rho(r) = P_c \rho_{core}(r) + P_v \kappa^3 \rho_{valence}(\kappa r) + \sum_{l=0}^{4} \kappa'^3 R_l(\kappa' r) + \sum_{m=-1}^{l} P_{lm} Y_{lm}(\frac{\vec{r}}{r})$$

where P_c, P_v and P_{lm} are population coefficients and $R_l(\kappa' r)$ is the slater type radial function, is a series expansion in real spherical harmonic functions through fourth order Y_{lm}. The parameters ρ_{core} and $\rho_{valence}$ can be constructed by using canonical Hartree – Fock atomic orbitals of the free atoms normalized to one electron and allowing the valence function to expand and contract by adjusting the variable parameters κ and κ'.

Table 2
Results of multipole refinement.

Oxidation state	Molecules	Atoms	Parameters			
			P_C	P_V	κ	κ′
+2	ZnO	Zn	18.2822	12.0239	0.9983	1.0000
		O	2.0502	5.8883	1.0156	1.0000
+3	Al_2O_3	Al	9.9808	2.4260	1.0296	1.0000
		O	2.0068	6.4154	0.9493	0.9618
+4	ZrO_2	Zr	36.0553	4.0333	0.9930	1.0000
		O1	2.0030	5.9884	1.0051	1.0000
		O2	1.9972	6.5086	0.9345	1.0000
+5	V_2O_5	V	18.0000	5.0074	0.9990	1.0000
		O1	2.2205	6.3605	0.9947	1.0000
		O2	1.9261	6.4008	0.9453	0.9013
		O3	2.1450	6.5108	0.9138	1.0000
+6	$WO_{3.333}H_{0.667}$	W1	54.2081	20.6186	0.9116	1.0000
		W2	54.1088	19.0946	1.1036	1.0000
		O1	1.9792	5.3939	1.1036	1.0000
		O2	1.9437	5.7840	1.3335	1.0000
		O3	1.8943	5.8478	1.5214	1.0000
		O4	1.5254	6.5500	0.8718	1.0000
		O5	2.4845	5.1170	1.0945	1.0000
		H	0.0000	0.9322	1.1459	1.0000

The same software JANA 2006 [56], which is used for rietveld refinement, is again used for multipole refinement of core, valence and pseudo-atomic electron occupancies P_{lm}. According to Hansen and Coppens [57], the neutral atom wave functions are extracted from Clementi tables [58] and the Slater type radial functions are used with $n_l = 4468$ for Zn/Zr/V, $n_l = 4446$ for Al, $n_l = 6668$ for W, $n_l = 2223$ for O and $n_l = 1123$ for H for $l \leq 4$. For individual atoms H, O, Al, V/Zn, Zr and W, the core charges are taken as He, Ne, Ar, Kr, Xe and Rn respectively during refinement and for all these atoms, the valence expansion/contraction parameter (κ) is refined in the five data sets. The results of the refinement are given as Table 2. The values greater than unity for the parameters κ and κ' indicate the contraction of the particular atoms and those less than unity indicate the expansion of that particular atoms. In this basis, the κ values in the table show that the

Table 1
Results of refinements.

Structure refinement using Rietveld technique						
Oxidation state	+1	+2	+3	+4	+5	+6
Parameters	SrO [30]	ZnO	Al_2O_3	ZrO_2	V_2O_5	$WO_{3.333}H_{0.667}$
a (Å)	5.1602	3.2472	4.7599	5.1522	11.5454	7.3304
b (Å)	5.1602	3.2472	4.7599	5.2139	3.5722	12.5237
c (Å)	5.1602	5.2017	12.9957	5.3208	4.3859	7.7085
Cell Volume ($Å^3$)	137.40	47.5007	254.9857	141.0885	181.0950	707.6603
Density (gm/cc)	4.7000	5.6879	3.9840	5.7990	3.3354	6.6975
U_{iso} ($Å^2$) (M)	–	0.0170	0.0384	0.0372	0.0398	0.0370 0.0484
U_{iso} ($Å^2$) (O)	–	0.0163	0.0014	0.0414 0.0402	0.0510 0.0196 0.0188	0.0412 0.0128 0.0222 0.0121 0.1326
U_{iso} ($Å^2$) (H)	–	–	–	–	–	0.0379
R_{obs} (%)	–	1.59	1.68	1.09	1.21	0.78
wR_{obs} (%)	–	2.80	2.55	1.59	1.79	1.46
Charge density by MEM refinement						
Lagrange parameter	0.019	0.0216	0.1235	0.0027	0.0205	0.0112
Number of cycles	1191	73	148	2753	311	11231
Prior electron density (e/$Å^3$)	1.3390	1.5999	1.1765	1.5877	0.9509	1.7183
Resolution (e$Å^{-3}$/pixel)	0.0863	0.051	0.075	0.081	0.056	0.075
R_{obs} (%)	1.02	1.55	1.66	1.03	1.59	1.90
wR_{obs} (%)	1.08	2.03	2.66	1.59	1.95	2.04

atoms Zn, Zr and V have undergone expansion while the Al atom has undergone contraction in ZnO, ZrO_2, V_2O_5 and Al_2O_3 systems respectively. The oxygen atom has undergone contraction in ZnO, but it has undergone expansion in Al_2O_3 and V_2O_5. This refinement has contributed two interesting results. One is that, in Zirconia, which has two oxygen sites, O1 atom which has a κ value of 1.0051, is found to get contracted whereas O2 atom with the κ value of 0.9345 is found to get expanded while bonding. The second interesting result is that, in tungsten trioxide hydrate, one among the two tungsten sites, W1 (for which, $\kappa = 0.9116$), expands whereas, the other site atom W2 (for which, $\kappa = 1.1036$), contracts. And also, in the same system, all oxygen atoms contract, except O4, which expands as its κ value (0.8718) is less than unity, while bonding. These effects reflect in the values of core (P_c) and valance (P_v) charges of all the atoms. For example, in ZnO, the sum of the values of P_c and P_v of Zn and O is 30.3061 and 7.9385 respectively. These values, when compared to the actual Z values of Zn (30) and O (8) confirm the expansion and contraction of the respective atoms. Nevertheless, since the shape of the valence charges is completely aspherical, κ' would be very difficult to refine.

To visualize the effect of temperature on charge distribution in the systems, the deformation density maps, in which the density of deformation is characterized as,

$$\Delta\rho_{multipole-deformation}(\overrightarrow{r}) = \frac{1}{V}\sum [F(\overrightarrow{h})_{multipole} - F(\overrightarrow{h})_{spherical-atom}]\exp[-2\pi i(\overrightarrow{h} - \overrightarrow{r})]$$

where $F_{multipole}$ represents the Fourier transform of the multipole electron density with or without convolution of thermal contribution, are constructed (Fig. 2). The fourier components are terminated at the experiment resolution. Here, the dynamic deformation maps indicate the convoluted form whereas the static deformation maps indicate the deconvoluted form of thermal contribution. All atoms show less deformation in the maps. Moreover, lone pair electrons of oxygen atoms are clearly visible in the figures.

The topological view of the charge distribution facilitates the investigation of general electron distribution pattern and offers a quantitative description of the bonding mechanism in the systems. Hence, based on the “Atoms In Molecules (AIM) theory” proposed by Bader [59], the charge distribution constructed using multipole model is analysed. According to him, “two atoms are bonded if they are connected by a line of maximum electron density called a bond path, on which lies a bond critical point (BCP) where $\overrightarrow{\nabla}\rho(r_{BCP}) = 0$, and the critical points are the characteristics of the bond existing between the atoms”.

Using Newton-Raphson method, the (3,-1) bond critical points are found in the place between every pair of neighboring nuclei and presented as Table 3. In the table, the distance between the metal atom - ligand atom, metal atom - CP and CP - ligand atom are represented by d, d_1, d_2 respectively. A (3,-1) CP with one positive eigen value corresponds to a saddle point of ρ as given in the table. According to Tsierelson [60], this electron density at the bond critical point serves as a tool to distinguish each atomic interaction types. Consequently, the interactions are categorized as closed shell atomic interactions ($\rho\ (bcp) < 0.3$ e/Å^3), intermediate interactions ($0.3 < \rho\ (bcp) < 1$ e/Å^3) and shared shell interactions ($1 < \rho\ (bcp) < 2$ e/Å^3) [60–63]. For +1 oxidation state of metal, the charge density at the bond critical point of the molecule SrO, which falls in to the category of ionic bonding, as reported by Israel et al. [30], is also included in the table.

G.C.Zhou et al. [51] performed a theoretical topological analysis of wurtzite ZnO and derived the CP values from LDA and GGA methods. These results strongly underestimated the symmetries of oxygen atoms. On the contrary, the present experimental topological analysis shows that in ZnO, which possess a single oxygen site, the oxygen atoms at two different symmetries exhibit two different bonding characteristics with Zn atoms, one points out a closed shell interaction, corresponding to a ρ value of 0.0766 e/Å^3 and the other points out an intermediate interaction, corresponding to a ρ value of 0.5672 e/Å^3. In corundum, which also possess a single oxygen site, even though the electron densities at the critical points of the bonds formed between the metal atom and the ligand atom at (x-y, x, -z) and that at (-y+1/3, x-y+2/3, z+2/3) differs, both the interactions are of intermediate type. In case of Zirconia, the values of the density of charges at the CP of bonds formed between Zr and its surrounded three O1 atoms are greater than unity, while, that of the bonds formed between Zr and its surrounded four O2 atoms are less than unity. This confirms that, the Zr atoms when bonded to O1 atoms, exhibit polar covalent characteristics, but the same when bonded to O2 atoms exhibit intermediate characteristics. Xilin Yin et al. [64] reported on the least ionic behavior of the singly coordinated vanadyl oxygen atom (O1), while bonded with vanadium atom, by performing density functional calculations in the bulk system, V_2O_5. The present experimental work also, reflects the least ionic behavior of the O1 oxygen atom through a very high ρ value of 3.3899 e/Å^3, when compared with the other doubly coordinated (O2) and triply coordinated (O3) atoms. This high value of ρ is beyond the Tsierelson's classification of interactions and hence it is classified under strong correlation induced bond. One another strong correlation induced bond is found between the O2 atom and the vanadium atom, as its electron density at the saddle is also very high (3.1364 e/Å^3). According to the density functional calculations [64], the degree of ionicity between the V atom and the O atoms decreased in the order: $O3 > O2 > O1$. In our work also, the decrease in the degree of ionicity between the metal and the ligand atoms is found to satisfy the same trend. Moreover, the table shows that among the two O3 atoms, bonded to the V atom, one has an intermediate characteristic (ρ= 0.5715 e/Å^3) and the other has a shared shell characteristic (ρ= 1.0794 e/Å^3), with respect to its symmetries. In case of the tungsten trioxide hydrate, all oxygen atoms, except the O1 atom at the symmetry (-x, -y+1/2, z+1/2), when bonded to W1 atom shows a high covalent behavior than those bonded to W2 atoms. Here also, the bonding characteristics differ with respect to the symmetries of the oxygen atoms. In case of O1 and O2 atoms, considering the dissimilar symmetries, the interactions are same with slight difference in bond length as well as ρ values. But, in view of O3 atoms, the bonding fluctuates between polar covalent (ρ= 1.5080 e/Å^3) and strong correlation induced (ρ= 3.9604 e/Å^3) depending on the symmetry.

This detailed topological analysis confirms a mixed ionic and covalent nature of bonding in all the systems. For a more lucid interpretation, the oxidation state of the metal is plotted against electron density at bcp, bond length and bonding radius of oxygen (Fig. 3). The general and well known fact about bonds is that, within a unit cell, the shortest bond is the strongest and the best possible bond in a molecule, because of its perfect geometrical arrangement of charges in that bonds. Hence the shortest bond in each interaction type is taken in to account. At low oxidation state of metals, the low ρ values (less than 0.3 e/Å^3) and high d values in the Fig. 3(a) and (b) indicate that the bonds are predominantly ionic and very weak. The bonding radius of oxygen is also high (Fig. 3(c)). The increase in oxidation state of cations, increases the importance of covalent character in bonds which is signified by the raise in the electron density at the critical point. Hence, from +2 oxidation state of cation, interactions between the metal and ligand atoms are intermediate, whereas from +4 oxidation state of cation, the interactions are both intermediate and polar covalent. As a result, the strength of the bonds also increases, as medium bonds for intermediate interactions and strong bonds for polar covalent interactions. As the charges from the ligand atom take part in covalent bonding formation, its bonding radius in intermediate interactions are comparatively low than that in closed shell interactions. And also, the same that in shared shell interactions are still low. At very high oxidation state of cations, i.e. at +5 and + 6 states, the electron density at the saddles of certain bonds is very high, declaring the presence of strong correlation induced bonds. Actually, in these systems, the charges that were originally present in covalent bond is shared in strong correlation induced bonds.

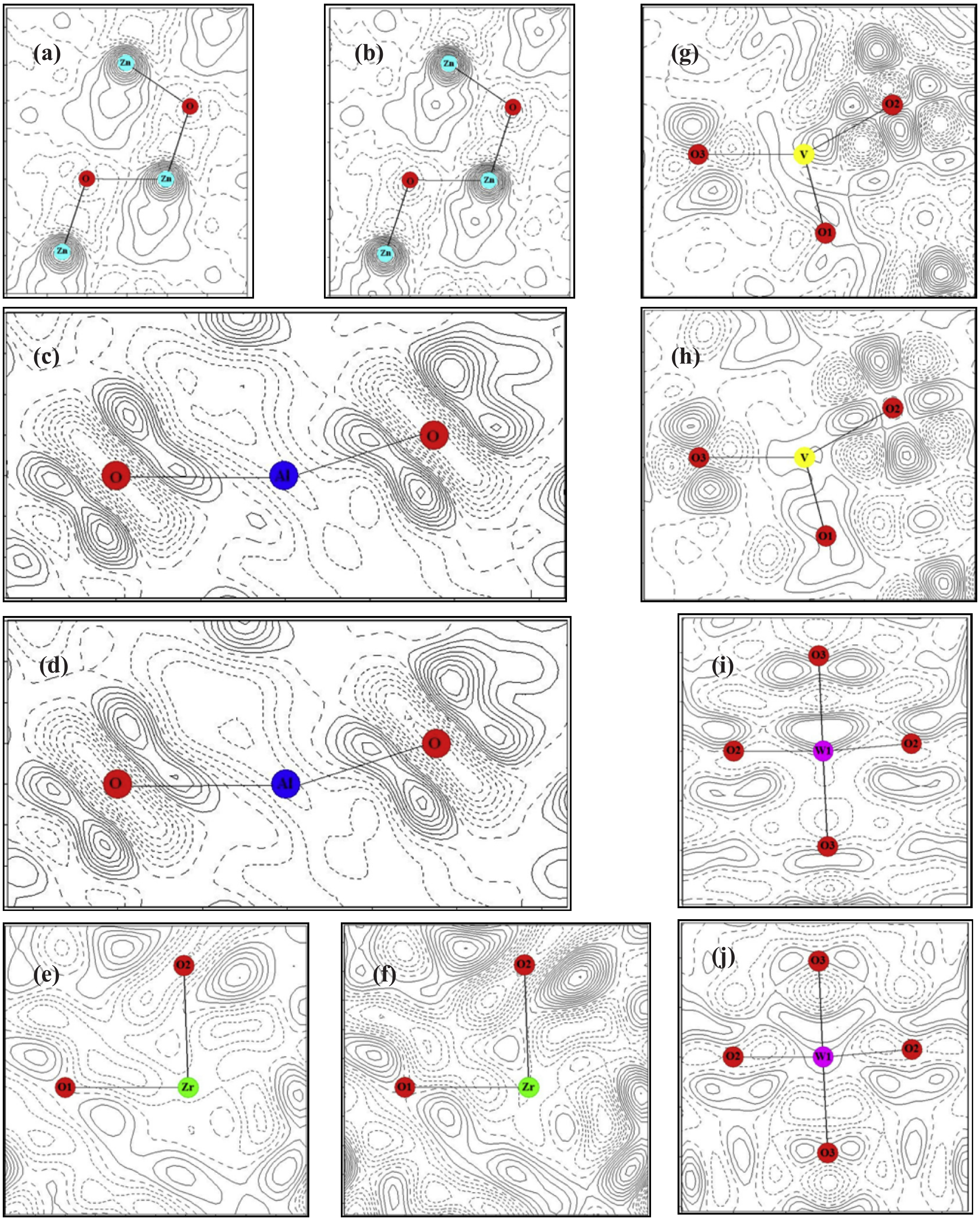

Fig. 2. Dynamic and static deformation multipole density maps of (a,b) ZnO, (c,d) Al_2O_3, (e,f) ZrO_2, (g,h) V_2O_5 and (i,j) $WO_3.1/3H_2O$ respectively. Negative contours are shown with dashed lines.

This reduces the charges at bcp of covalent bonds in those chosen molecules. Part of the charges reduced in covalent bond is taken care of by the strongly correlated bonds. And also, most of the charges will be at the bond path of these strongly correlated bonds and hence the electron densities at bond critical points of these bonds increase with increase in oxidation state of metal. Fig. 3(b) shows that the medium and strong bonds are getting stronger at high oxidation state of metals. Shrinking of bond lengths are evidenced in case of strong correlation induced interactions. This authenticates that strongly correlated bonds are the strongest bonds. Perhaps, the increase in bond length of strong correlation induced bond in +6 oxidation state, i.e. in $WO_{3.333}H_{0.667}$, is due to the involvement of H atom and the presence of $O_{3.333}$ instead of O_3. The bonding radius of oxygen in strongly correlated interactions are comparatively low than that in other interactions. Thus this graph serves as the most important step for the purpose of this paper, as it illustrates the degree of the involvement of covalency and strong correlation in binary oxides with respect to oxidation state of metals.

4.2. MEM analysis

The refined structure factors are further used for MEM analysis, a statistical and probabilistic approach of charge density. Maximum entropy method (MEM), as proposed by Collins [65], serves as an exact tool to obtain the valence charge density along the bond path through high resolution density distribution maps. Initially, the unit cells of all the systems are divided so as to contain 64 × 64 x 102 pixels in ZnO, 64 × 64 x 174 pixels in Al_2O_3, 64 × 65 x 66 pixels in ZrO_2, 207 × 64 x 79 pixels in V_2O_5 and 64 × 109 x 67 pixels in $WO_{3.333}H_{0.667}$ in

Table 3
(3,-1) bond critical points.

Oxidation state	Molecules	Bond	Symmetry	Mem	Multipole			Tsirelson's classification of BCP, ρ (e/Å^3)			Strong Correlation induced interactions
				d (Å)	d (Å)	d_1 (Å)	d_2 (Å)	Ionic interactions	Intermediate interactions	Polar covalent interactions	
+1	SrO [30]	Sr–O	–	2.5801	–	1.1501	1.4300	0.0400	–	–	–
+2	ZnO	Zn–O	Zn – (-x, -y, z+1/2) O – (-x, -y, z+1/2) Fig. 3(a)	2.0008	2.0008	1.1663	0.8345	0.0766	–	–	–
		Zn–O	Zn – (-x, -y, z+1/2) O – (x, y, z) Fig. 3(a)	2.0678	2.0679	1.1303	0.9376	–	0.5672	–	–
+3	Al_2O_3	Al–O	Al – (y+1/3, x+2/3,-z+1/6) O – (-y+1/3, x-y+2/3, z+2/3)Fig. 4(a)	2.0089	2.0089	1.2552	0.7537	–	0.3439	–	–
		Al–O	Al – (y+1/3, x+2/3,-z+1/6) O – (x-y, x, -z) Fig. 4(a)	1.9162	1.9161	1.2201	0.6960	–	0.6098	–	–
+4	ZrO_2	Zr–O1	Zr – (-x, y+1/2,-z+1/2) O1 – (-x, -y, -z) Fig. 5(a), (c)	2.2562	2.2561	1.2117	1.0444	–	–	1.3283	–
		Zr–O1	Zr –(-x, y+1/2, -z+1/2) O1 –(-x, y+1/2, -z+1/2) Fig. 5(b)	2.0427	2.0427	1.1257	0.9170	–	–	1.2337	–
		Zr–O1	Zr – (-x, y+1/2, -z+1/2) O1 – (x, y, z) Fig. 5(d)	2.0464	2.0464	1.0420	1.0044	–	–	1.0876	–
		Zr–O2	Zr – (-x, y+1/2, -z+1/2) O2 – (-x, -y, -z) Fig. 5(a)	2.3058	2.3059	1.2346	1.0713	–	0.4001	–	–
		Zr–O2	Zr – (-x, y+1/2, -z+1/2) O2 – (x, y, z) Fig. 5(b)	2.2013	2.2012	1.1391	1.0621	–	0.6257	–	–
		Zr–O2	Zr – (-x, y+1/2, -z+1/2) O2 – (x, -y+1/2, z+1/2) Fig. 5(c)	2.3200	2.3201	1.3167	1.0034	–	0.4902	–	–
		Zr–O2	Zr – (-x, y+1/2, -z+1/2) O2 – (-x, y+1/2, -z+1/2) Fig. 5(d)	2.1108	2.1108	1.1107	1.0001	–	0.9616	–	–
+5	V_2O_5	V–O1	V – (-x+1/2, y+1/2, -z) O1 – (-x+1/2, y+1/2, -z) Fig. 6(a)	1.4100	1.4101	0.9277	0.4824	–	–	–	3.3899
		V–O2	V – (-x+1/2, y+1/2, -z) O2 – (-x+1/2, y+1/2, -z) Fig. 6(a)	1.8700	1.8700	0.9868	0.8832	–	–	–	3.1364
		V–O3	V – (-x+1/2, y+1/2, -z) O3 – (-x+1/2, y+1/2, -z) Fig. 6(a)	2.0286	2.0285	1.1933	0.8352	–	0.5715	–	–
		V–O3	V – (-x+1/2, y+1/2, -z) O3 – (x, y, z) Fig. 6(b)	1.9111	1.9110	1.1808	0.7302	–	–	1.0794	–
+6	$WO_{3.333}H_{0.667}$	W1–O1	W1 – (-x, -y+1/2,z+1/2) O1 – (x+1/2, y, z+1/2) Fig. 7(b)	1.9673	1.9673	0.9871	0.9802	–	0.7196	–	–
		W1–O1	W1 – (-x, -y+1/2,z+1/2) O1 – (-x, -y+1/2, z+1/2) Fig. 7(b)	1.9672	1.9672	0.9886	0.9786	–	0.5673	–	–
		W1–O2	W1– (-x, -y+1/2, z+1/2) O2 – (-x, -y+1/2, z+1/2) Fig. 7(a)	1.8653	1.8653	0.9719	0.8934	–	–	1.0590	–
		W1–O2	W1– (-x, -y+1/2, z+1/2) O2 – (x+1/2, y, z+1/2) Fig. 7(a)	1.8654	1.8654	0.9128	0.9526	–	–	1.1193	–
		W1–O3	W1 – (-x, -y+1/2,z+1/2) O3 – (-x, -y+1/2, z+1/2) Fig. 7(a)	1.7331	1.7330	0.9860	0.7470	–	–	–	3.9604
		W1–O3	W1 – (-x, -y+1/2,z+1/2) O3 – (-x, y, z) Fig. 7(a)	1.9295	1.9295	1.4430	0.4865	–	–	1.5080	–
		W2–O2	W2 – (x, y+1/2, z+1/2) O2 – (-x, y+1/2, z+1/2) Fig. 7(c)	2.1719	2.1719	1.1151	1.0568	–	0.6270	–	–
		W2–O5	W2 – (x, y+1/2, z+1/2) O5 – (x, y+1/2, z+1/2) Fig. 7(d)	1.8502	1.8502	0.8603	0.9899	–	0.4099	–	–

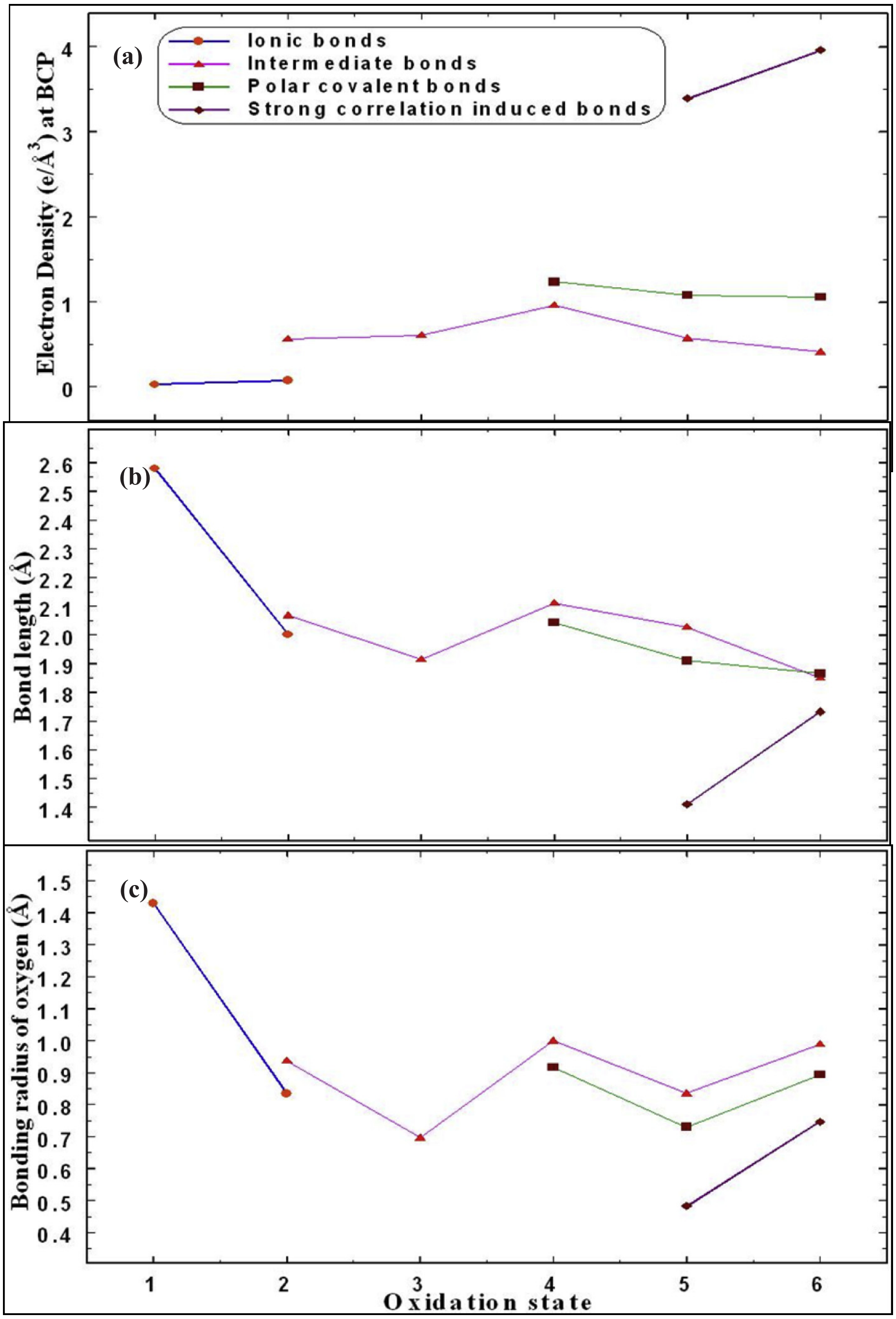

Fig. 3. Oxidation state versus (a) electron density at bcp, (b) bond length and (c) bonding radius of oxygen.

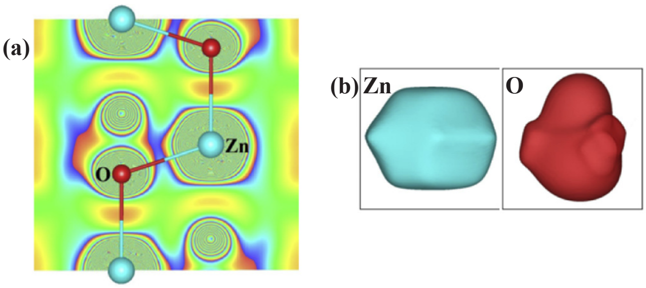

Fig. 4. (a) Two-dimensional electron density map and (b) atomic basins of ZnO.

accordance with their ratio of cell dimensions along the three crystallographic axes. To evaluate the electron density, the principle of this method is to maximize the entropy in an iterative cycle in the i th pixel in a unit cell in terms of the assumed uniform prior density at that pixel, subject to the constraint,

$$C = \frac{1}{N}\sum_{k}\frac{|F_{obs}(k) - F_{cal}(k)|^2}{\sigma^2}$$

that compares the observed and calculated structure factor, as proposed by Sakata and Sato [66]. Here N, $F_{Obs}(k)$, $F_{Cal}(k)$ and σ denotes the number of reflections, observed and calculated structure factors and standard deviation respectively. The entropy becomes maximum when C tends to unity and hence results in the desired electron density,

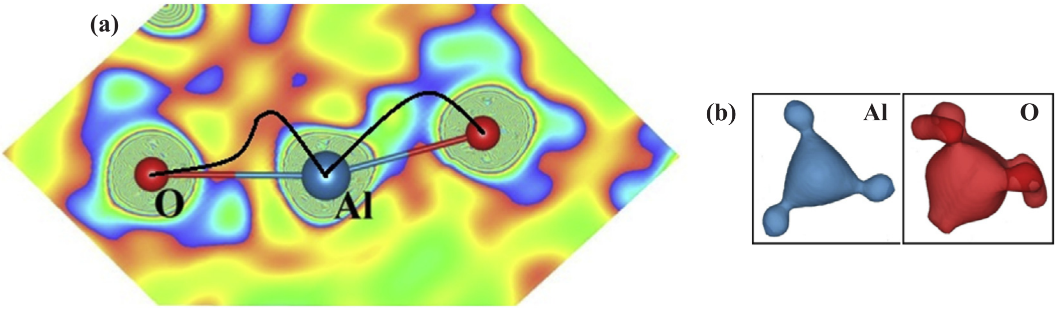

Fig. 5. (a) Two-dimensional electron density map and (b) atomic basins of Al_2O_3.

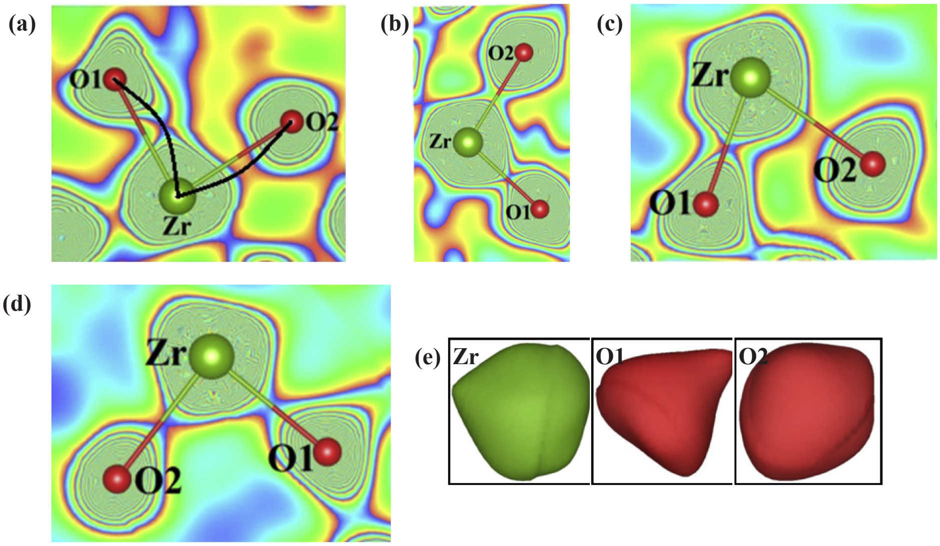

Fig. 6. (a), (b), (c) and (d) Two-dimensional electron density maps and (e) atomic basins of ZrO_2.

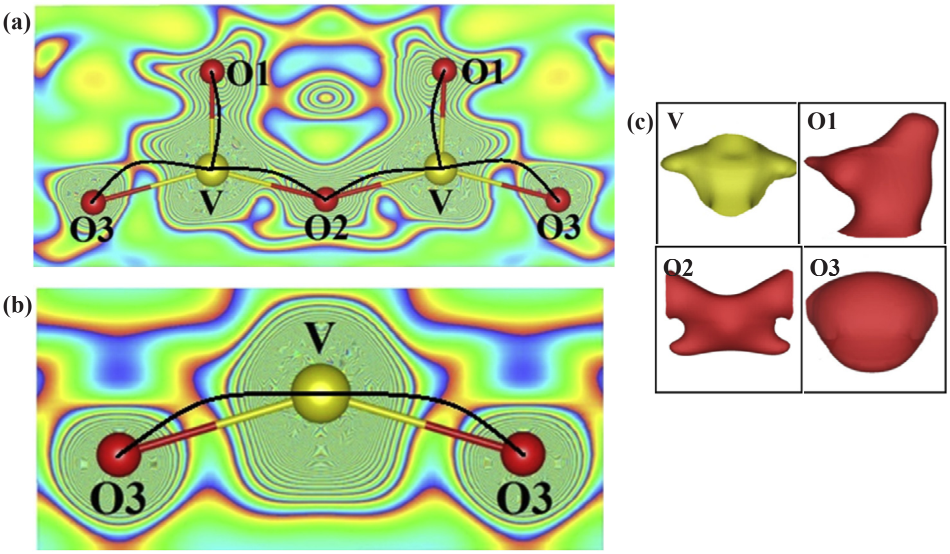

Fig. 7. (a) and (b) Two-dimensional electron density maps and (c) atomic basins of V_2O_5.

$$\rho_{MEM}(r_i) = \tau(r_i)\exp[(\frac{\lambda F_{000}}{N})\sum[1/\sigma(k)]^2|F_{Obs}(k) - F_{Cal}(k)|\exp(-2\pi j\, k.r)]$$

where $\tau(r_i)$ is the prior electron density and F_{000} is the number of electrons in the unit cell. The software PRIMA [67,68], which employs this method is used for computation. The prior charge density (F_{000}/V) assigned to each pixel, the number of iterative cycles carried out for each system and several other parameters resulted in refinement are given in Table 1. The low reliability indices in the table reveal the high quality nature of the five available data sets.

This maximum entropy method compliments three necessary tools for bonding investigations, 3-D and 2-D charge density distribution maps and 1-D charge density profiles. For this purpose, the resultant

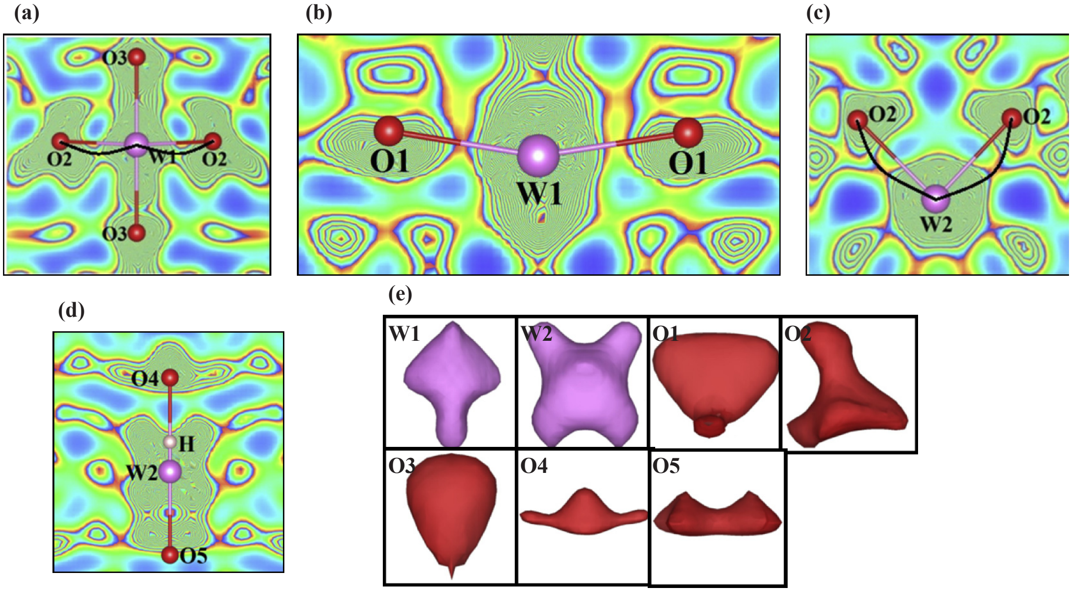

Fig. 8. (a), (b), (c) and (d) Two-dimensional electron density maps and (e) atomic basins of $WO_3.1/3H_2O$.

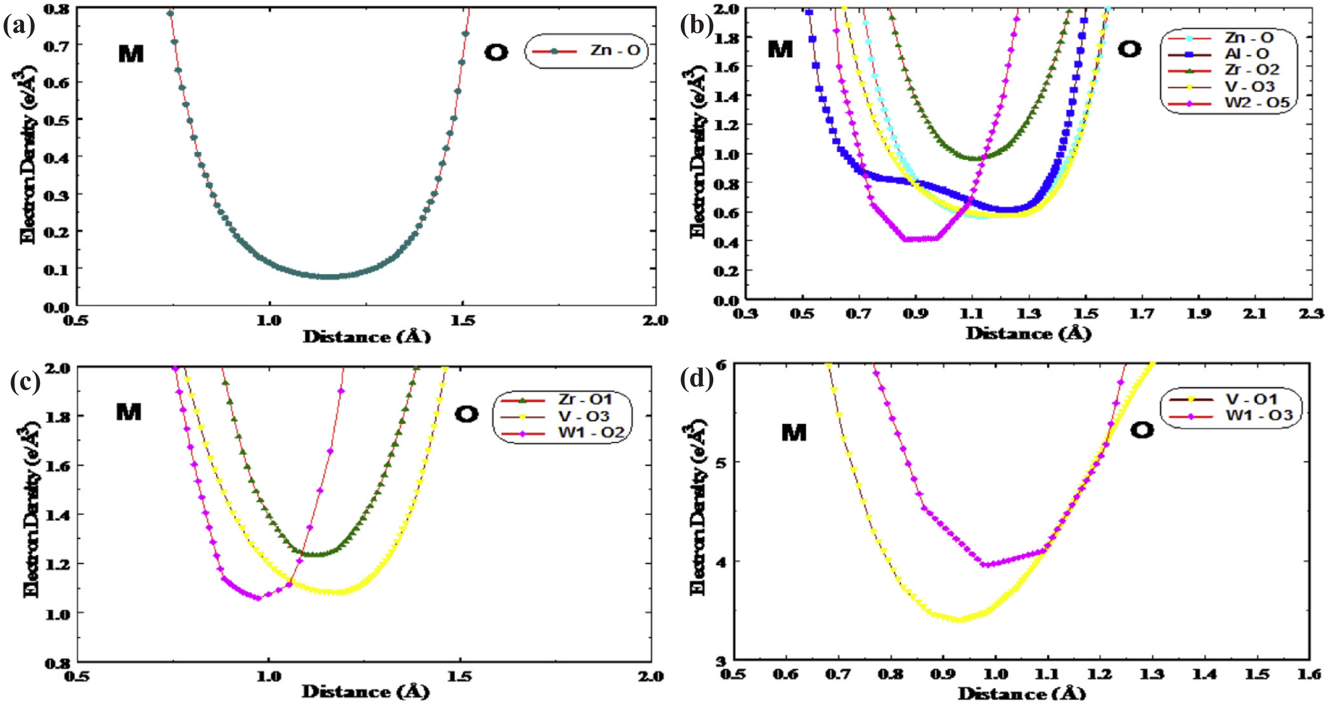

Fig. 9. One dimensional charge density profiles of (a) Ionic, (b) Intermediate, (c) Polar covalent, and (d) Strong correlation induced bonds.

charge density is plotted and visualized by using the software VESTA [69]. The three dimensional arrangement of charges in the unit cell were mapped in ball and stick model of structure and the maps showed very clear and highly resolved electron clouds in some areas and covalent charge gathering over some other areas. Moreover, certain interesting and at the same time important points are noticed. In almost all the systems, the ligand atoms of same site exhibit various bonding characteristics depending on its symmetry. This is a prime evidence for the results discussed in topological analysis.

This creates a necessity, to map and study the 2-D profiles along various bonding planes so that all these bond paths are clearly understood. And also, in order to have a specific visualization of the density variations in the bonding regions, two dimensional maps are plotted (Figs. 4(a), 5(a), 6(a)–(d),7(a) and (b) and 8(a)–(d)) in BGR (Blue Green Red) scale. The saddle regions with blue shade indicate high density whereas those with red shade indicate a comparative low density. This helps the bonding criteria to be more visible and clear to understand. In Figs. 4(a) and 5(a) i.e. in ZnO and Al_2O_3 systems, the oxygen atoms enacting two different behaviours in bonding are well pronounced, through red saddles representing low density and blue saddles representing comparative high density. This authenticates the same argument in topological analysis in case of these two systems. The curved bond paths are also clearly seen in the latter case. In the two dimensional plots of ZrO_2 (Fig. 6(a), (b), (c) and (d)), the polar covalent bonds formed by Zr atom when interacted with O1 atoms are characterized by blue saddles. A keen observation in to these figures clearly show the symptoms of electron sharing between the metal atom and the ligand atoms for which the value of $\rho \geq 1$. In the 2-D mem maps of V_2O_5

(Fig. 7(a)) and $WO_{3.333}H_{0.667}$ (Fig. 8(a)), the strongly correlated bonds are evidenced as discussed in topological analysis. And also, from the Fig. 7(a) and (b), there is no doubt that, in vanadium pentoxide, the ionic character decreases in the order: $O3\,(red\ saddle) > O2(green\ saddle) > O1(blue\ saddle)$. The fact that the O1 ligand is the least ionic, once again reflects here. In $WO_{3.333}H_{0.667}$ (Fig. 8(d)), the position of hydrogen atom is clearly picturized in between W2 atom and O4 atom. This confirms that O4 is a water molecule as reported by Gerand et al. [49]. Owing to the inclusion of H atom in the other end of the bond (i.e. in between W2—O4 bond), for charge balance, the W2—O5 bond gets very weak with a low mid bond density of 0.4099 e/$Å^3$. The curved bond paths are specified in the figures. The bond lengths (given in Table 3) and density at the mid bonds derived from MEM analysis matches very well with the same derived from multipole analysis.

The two dimensional maps of all the systems clearly exhibit the aspherical nature of both the metal and ligand atoms, while bonding. Hence, for the close investigation of this asphericity, true valence charge density figures encapsulating atomic basins (regions of space which is enclosed inside a zero charge density flux surface, $\vec{\nabla}\rho\cdot\vec{n}$, where $\vec{n}$ is the unit vector of surface) are drawn (Figs. 4(b) and 5(b), 6(e), 7(c) and 8(e)). The figures explicitly disclose the fact that the atomic basins of the atoms are not influenced by the symmetries and bonding natures of the atoms and obviously, it depend on the site of that particular atom.

Charge densities at BCPs and the quantified transfer of charge are the two necessary tools to discuss in the course of study of bonding features. Hence the atomic charges are calculated by using the method of numerical integration of the electron density over zero flux atomic basins in all the molecules. This calculation of basin integration in Zirconia showed a transfer of 3.9202e from the Zr atom to both the three O1 and four O2 ligands: 0.9032e are associated with each O1 atom, while 0.3026e are transferred to each O2 ligand. Except baddeleyite, in which the atomic basins of both Zr and O are very close to spherical shape (Fig. 6(e)), the integration of charge could not lead to successful results for the remaining four molecules. For other atoms, the basins deviate from spherical surface (Figs. 4(b), 5(b), 7(c) and 8(e)). Indeed, clear definitions of zero flux surfaces are not possible in many of the atoms having small surface. Also, the oxygen shapes go aspherical in all the cases. This makes it difficult to define a near spherical or zero flux surface and hence the charge integration becomes very difficult for these cases. All these arguments may be the reasons for the difficulties in the calculation of charge transfer in the remaining systems. However, the interactions between metal and oxygen atoms, through charge density plots, prove that the potential of shared shell and strong correlation interactions increases with the increase in oxidation state of metals.

To quantify the MEM 3-D and 2-D results, one dimensional charge density profiles are drawn along all the shortest ionic, intermediate, polar covalent and strong correlation induced bonds and presented as Fig. 9. The exact values of charges at the saddle points match very well with the values in Table 3. In the figure, the profiles of the systems with high oxidation state of cation are shallower than that with low oxidation state of cation. This shows an increase in shared charge accumulation in the bonding regions of the former than the latter. Hence our conclusion from this investigation of oxygen bonding with respect to the ascending order of the oxidation state of metal cations is that, at low oxidation states the ionic character of bonding predominates in binary oxides. As the oxidation state increases, gradually, the intermediate and then the polar covalent interactions are found to be taking up. Ultimately, it reaches the strong correlation induced interactions along with the intermediate and polar covalent interactions. In all the molecules, intermediate type of bonding characteristics is evidenced.

5. Conclusion

The present work collects into one place the relevant pieces of information about the bonding properties of certain transition and post transition binary metal oxides using charge density analysis. A qualitative as well as quantitative analysis of electron densities along different bonding planes is substantiated. This study clearly reveals that these systems exhibit iono-covalent character, and also, the covalent nature of bonding increases with increase in the oxidation state of metals. Except SrO, which is purely ionic, all the compounds show evidences of intermediate type of bonding. At high oxidation states, strongly correlated bonds are also recognized. Such studies in more oxides are needed to remove the inadequacy of understanding the bonding principles in these captivating materials.

References

[1] J.L.G. Fierro, Metal Oxides: Chemistry and Applications, CRC Press, 2005.
[2] Hari Singh Nalwa, Handbook of Surfaces and Interfaces of Materials, Five-volume Set, Academic Press, 2001.
[3] P.D.C. King, T.D. Veal, A. Scleife, J. Zuniga-Perez, B. Martel, P.H. Jefferson, F. Fuchs, V. Munoz-Sanjose, F. Bechstedt, C.F. McConville, Valence-band electronic structure of CdO, ZnO, and MgO from x-ray photoemission spectroscopy and quasi-particle-corrected density-functional theory calculations, Phys. Rev. B 79 (2009) 205205.
[4] M. Veronica Ganduglia-Pirovano, Alexander Hofmann, Joachim Sauer, Oxygen vacancies in transition metal and rare earth oxides: current state of understanding and remaining challenges, Surf. Sci. Rep. 62 (2007) 219–270.
[5] C.N.R. Rao, II. Transition metal oxides (including cuprate superconductors), Annu. Rev. Phys. Chem. 40 (1989) 291–326.
[6] S.K. Deb, Physical properties of a transition metal oxide: optical and photoelectronic properties of single crystal and thin film molybdenum trioxide, Proc. Roy. Soc. A 304 (1968) 211–231.
[7] SivachandranBalendran SumeetWalia, Hussein Nili, Serge Zhuiykov, Rosegarten Gary, Qing Hua Wang, SharathSriram MadhuBhaskaran, Michael S. Strano, KouroshKalantar-zadeh, "Transition metal oxides – thermoelectric properties", Prog. Mater. Sci. 58 (8) (2013) 1443–1489.
[8] Linus Pauling, The nature of the chemical bond. IV. The energy of single bonds and the relative electronegativity of atoms, J. Am. Chem. Soc. 54 (1932) 3570–3582.
[9] Victor E. Henrich, P.A. Cox, The Surface Science of Metal Oxides, Cambridge University Press, 1996.
[10] Victor E. Henrich, Metal oxide surfaces and interfaces: concepts and issues, Book – "The Chemical Physics of Solid Surfaces : Oxide Surfaces, vol. 9, Elsevier Science, 2001.
[11] R. Saravanan, M. Prema Rani, Metal and Alloy Bonding: an Experimental Analysis, Springer-Verlag London Limited, 2012.
[12] Linus Pauling, The principles determining the structure of complex ionic crystals, J. Am. Chem. Soc. 51 (1929) 1010–1026.
[13] Robert S. Mulliken, A new electroaffinity scale; Together with data on valence states and on valence ionization potentials and electron affinities, J. Chem. Phys. 2 (1934) 782.
[14] Robert S. Mulliken, Electronic structures of molecules. XI.Electroaffinity, molecular orbitals and dipole moments, J. Chem. Phys. 3 (1935) 573.
[15] A.L. Allred, E.G. Rochow, A scale of electronegativity based on electrostatic force, J. Inorg. Nucl. Chem. 5 (1958) 264–268.
[16] A.L. Allred, Electronegativity values from thermochemical data, J. Inorg. Nucl. Chem. 17 (1961) 215–221.
[17] R.T. Sanderson, Electronegativity and bond energy, J. Am. Chem. Soc. 105 (8) (1983) 2259–2261.
[18] R.T. Sanderson, Polar Covalence, Academic Press, New York, 1983.
[19] C. Leland, Allen, "Electronegativity is the average one - electron energy of the valence – shell electrons in ground – state free atoms", J. Am. Chem. Soc. 111 (1989) 9003–9014.
[20] P. Hohenberg, W. Kohn, Inhomogeneous electron gas, Phys. Rev. 136 (1964).
[21] G. Robert, Parr and Weitao Yang, "Density- Functional Theory of Atoms and Molecules", Oxford University Press, 1989.
[22] M. Linglet, Iono-covalent character of the metal-oxygen bonds in oxides: a comparison of experimental and theoretical data, Active Passive Elec. Comp. 27 (2004).
[23] J.A. Duffy, Chemical bonding in the oxides of the elements: a new appraisal, J. Solid State Chem. 62 (1986) 145–157.
[24] H. Idriss, E.G. Seebauer, Effect of oxygen electronic polarisability on catalytic reactions over oxides, Catal. Lett. 66 (2000) 139–145.
[25] AndrzejStoklosa, "Molar Volume, Ionic Radii in Stoichiometric and Nonstoichiometric Metal Oxides",Stoichiometry and Materials Science - when Numbers Matter, Intech, 2012.
[26] Gianfranco Pacchioni, Carmen Sousa, FrancescIllas, FulvioParmigiani, S. Paul, Bagus, "Measures of iconicity of alkaline-earth oxides from the analysis of ab initio cluster wavefunctions", Phys. Rev. B 48 (16) (1993) 11573–11582.
[27] Gabriele Centi, Fabrizio Cavani, Ferrucio Trifiro, Selective Oxidation by Heterogeneous Catalysis, Springer Science and Business media, 2012.

[28] William W. Porterfield, “Inorganic Chemistry – a Unified Approach”, second ed., Academic press, Inc, 1984.

[29] Victor E. Henrich, Electronic Structure of Mineral Surfaces”, Book – “Physics and Chemistry of Mineral Surfaces, CRC press, 1996.

[30] S. Israel, R. Saravanan, N. Srinivasan, S.K. Mohanlal, An investigation on the bonding in MgO, CaO, SrO and BaO from the MEM electron density distributions, J. Phys. Chem. Solid. 64 (2003) 879–886.

[31] P.A. Cox, Transition Metal Oxides - an Introduction to Their Electronic Structure and Properties, Oxford University press, 1992.

[32] H.H. Kung, Transition Metal Oxides : Surface Chemistry and Catalysis, Elsevier Science Publishers B.V., 1989.

[33] J.M.D. Coey, M. Venkatesan, Hongjun Xu, “Introduction to Magnetic Oxides”, Book – “Functional Matal Oxides – New Science and Novel Applications”, Wiley – VCH, 2013.

[34] Joseph R. Smyth, Steven D. Jacobsen, Robert M. Hazen, Comparative crystal Chemistry of dense oxide minerals, Rev. Mineral. Geochem. 41 (2000) 157–186.

[35] V.A. Coleman, C. Jagadish, “Basic Properties and Applications of ZnO”, Book – “Zinc Oxide Bulk, Thin Film and Nanostructures, Processing, Properties and Applications”, Elsevier, 2006.

[36] Kin Mun Wong, S.M. Alay-e-Abbas, A. Shaukat, Yaoguo Fang, Yong Lei, “First – principles investigation of the size – dependent structural stability and electronic properties of O- vacancies at the ZnO polar and non-polar surfaces”, J. Appl. Phys. 113 (2013) 1–11 01434.

[37] Pengshou XU, Yuming SUN, Chaoshu SHI, Faqiang XU, Haibin PAN, Electronic structure of ZnO and its defects, Sci. Chin. (Series A) 44 (9) (2001) 1174–1181.

[38] W.Y. Ching, Yong Nian Xu, First – principles calculation of electronic, optical, and structural properties of $\alpha - Al_2O_3$, J. Am. Ceram. Soc. 77 (Issue 2) (1994) 404–411.

[39] J. Lewis, D. Schwarzenbach, Electric field gradients and charge density in corundum, $\alpha - Al_2O_3$, Acta Crystallogr. A38 (1982) 733–739.

[40] Takashi Shirai, Hideo Watanabe, Masayoshi Fuji, Minoru Takahashi, Structural properties and surface characteristics on Aluminium Oxide powders, Annual Report of the Ceramics Research Laboratory, vol. 9, Nagoya institute of technology, 2009, pp. 23–31.

[41] A.F. Lima, J.M. Dantas, M.V. Lalic, An ab-initio study of electronic and optical properties of corundum Al_2O_3 doped with Sc, Y, Zr and Nb, J. Appl. Phys. 112 (2012) 1–9 093709.

[42] Deane K. Smith, Herbert W. Newkirk, The crystal structure of baddeleyite (monoclinic ZrO_2) and it's relation to the polymorphism of ZrO_2, Acta Crystallogr. 18 (1965) 983–991.

[43] Yan Zhang, Vincent Ji, Ke-Wei Xu, The detailed geometrical and electronic structures of monoclinic Zirconia, J. Phys. Chem. Solid. 74 (2013) 518–523.

[44] Yi Zhang, Jing Zhang, First principles study of structural and thermodynamic properties of Zirconia, Mater. Today : Proceedings 1 (2014) 44–54.

[45] R. Enjalbert, J. Galy, A refinement of the structure of V_2O_5, Acta Crystallogr. C42 (1986) 1467–1469.

[46] J. Haber, M. Witko, R. Tokarz, Vanadium pentoxide I. Structures and properties, Appl. Catal., A : General 157 (Issues 1–2) (1997) 3–22.

[47] A. Chakrabarti, K. Hermann, R. Druzinic, M. Witko, F. Wagner, M. Petersen, Geometric and electronic structure of Vanadium pentoxide : a density functional bulk and surface study, Phys. Rev. B 59 (Number 16) (1999) 10583–10590.

[48] Elisa Londero, Elsebeth Schroder, Role of van der Waals bonding in the layered oxide V_2O_5 : first principles density - functional calculations, Phys. Rev. B 82 (2010) 1–8 054116.

[49] B. Gerand, G. Nowogrocki, M. Figlarz, A new tungsten trioxide hydrate, WO_3.1/3 H_2O : preparation, characterization, and Crystallographic study, J. Solid State Chem. 38 (1981) 312–320.

[50] S. Salmaoui, F. Sediri, Large-scale synthesis and electrochemical properties of hydrated tungsten trioxide-based hierarchical microstructures, J. Alloy. Comp. 661 (2016) 82–91.

[51] G.C. Zhou, L.Z. Sun, X.L. Zhong, Xiaoshuang Chen, Wei LU, J.B. Wang, First-principle study on bonding mechanism of ZnO by LDA + U method, Phys. Lett. 368 (2007) 112–116.

[52] Ghadah S. Alghamdi, Ali Z. Alzahrani, Bonding formation and orbitals nature of ZnO structure, Middle East J. Sci. Res. 13 (9) (2013) 1144–1149.

[53] M.Causa, R.Dovesi, C.Pisani, and C.Roetti, “Ab initio characterization of the (0001) and (101¯0) crystal faces of α-alumina”, Surf. Sci. 215, Issues 1–2, 259-271.

[54] J.E. Medvedeva, A.J. Freeman, C.B. Geller, D.M. Rishel, Screened-exchange determination of the electronic properties of monoclinic, tetragonal, and cubic Zirconia, Phys. Rev. B 76 (2007) 1–7 235115.

[55] H.M. Rietveld, A profile refinement method for nuclear and magnetic structures, J. Appl. Crystallogr. 2 (1969) 65–71.

[56] V. Petricek, M. Dusek, L. Palatinus, JANA 2006, the Crystallographic Computing System, Institute of Physics, Academy of sciences of the Czech republic Praha, 2000.

[57] N.K. Hansen, P. Coppens, Acta Crystallogr. A34 (1978) 909–921.

[58] E. Clementi, C. Roetti, Roothaan-Hartree-Fock atomic wave functions, At. Data Nucl. Tab. 14 (1974) 177–478.

[59] R.F.W. Bader, Atoms in Molecules—A Quantum Theory, Oxford Univ. Press, Oxford, 1990.

[60] V.G. Tsierelson, Acta Crystallogr. A55 (1999) Supplement, Abstract M 13-OF-003, (1999).

[61] Adam I. Stash, Kiyoaki Tanaka, Kazunari Shiozawa, Hitoshi Makino, Vladimir G. Tsirelson, Atomic interactions in ethylenebis (1-indenyl) zirconium dichloride as derived by experimental electron density analysis, Acta Crystallogr. B61 (2005) 418–428.

[62] S. Israel, K.S. Syed Ali, R.A.J.R. Sheeba, R. Saravanan, Analysis on experimental valence charge density in germanium at RT and 200K, J. Phys. Chem. Solid. 70 (2009) 1185–1194.

[63] S. Israel, K.S. Syed Ali, R.A.J.R. Sheeba, R. Saravanan, X-ray analysis of the charge density distribution in GaP at 296 and 200K using a multipole model and the maximum entropy method, Chin. J. Phys. 47 (No.3) (2009) 378–400.

[64] Xilin Yin, Adil Fahmi, Akira Endou, Ryuji Miura, Isao Gunji, Ryo Yamauchi, Momoji Kubo, Abhijit Chatterjee, Akira Miyamoto, Periodic density functional study on V_2O_5 bulk and (001) surface, Appl. Surf. Sci. 130–132 (1998) 539–544.

[65] M. Collins, Nature 298 (1982) 49.

[66] M. Sakata, M. Sato, Acta Crystallogr. A46 (1990) 263.

[67] R.A. Dilanian, F. Izumi, Super-fast Program, PRIMA, for the Maximum Entropy Method, (2005).

[68] F. Izumi, R.A. Dilanian, Recent Research Developments in Physics vol. 3, Transworld Research Network, Trivandrum, 2002, p. 699 Part II.

[69] K. Momma, F. Izumi, VESTA, “visualisation for electronic and structual analysis”, Comm. Crystallogr. Comput. IUCr Newslett. 7 (2006) 106.